International Journal of Impact Engineering 64 (2014) 91–100

Contents lists available at ScienceDirect

International Journal of Impact Engineering

journal homepage: www.elsevier.com/locate/ijimpeng

Numerical simulation of ultra high performance fibre reinforced concrete panel subjected to blast loading

Lei Mao [a,*], Stephanie Barnett [a], David Begg [a], Graham Schleyer [b], Gavin Wight [c]

[a] School of Civil Engineering and Surveying, University of Portsmouth, Portland Building, Portland Street, Portsmouth PO1 3AH, UK
[b] Department of Engineering, University of Liverpool, Brownlow Hill, Liverpool L69 3GH, UK
[c] VSL Infrastructure Protection Ltd, 25 Senoko Way, Woodlands East Industrial Estate, Singapore 758047, Singapore

ARTICLE INFO

Article history:
Received 23 May 2013
Received in revised form
19 September 2013
Accepted 3 October 2013
Available online 14 October 2013

Keywords:
Ultra high performance fibre reinforced concrete
Concrete damage model
Blast loads
Steel fibre
Steel reinforcement

ABSTRACT

In the last few decades, several full-scale blast tests have been performed to study the behaviour of ultra high performance fibre reinforced concrete (UHPFRC). However, only limited research has been devoted to simulate performance of UHPFRC subjected to blast loading. This paper presents a numerical investigation on the performance of UHPFRC under blast loading with a concrete material model which takes into account the strain rate effect. Furthermore, the model is modified to better express the strain softening of UHPFRC material. The performance of the numerical models is verified by comparing modelling results to the data from corresponding full scale blast tests. With the verified models, parametric studies are also carried out to investigate the effect of steel reinforcement and steel fibre in increasing UHPFRC resistance to blast loading.

1. Introduction

The behaviour of concrete structures under explosion loading is a topic of major concern in both civil and material engineering. With the strain rate effect, the concrete behaviour subjected to high strain rate loading will be different from that under static loading. In the last few decades, much research has been devoted to investigate concrete behaviour under high strain rate loading using both experimental and numerical studies [1–4]. Moreover, due to the brittle nature of concrete materials, several methods have been developed to further increase the concrete resistance to high strain rate loading, such as adding fibre reinforcement to the concrete or use of high strength concrete materials [5–9].

Ultra high performance fibre reinforced concrete (UHPFRC) is a concrete material with both high strength concrete and fibre reinforcement. It has high cement content and low water/cement ratio. Fine silica sand and short steel fibres are also included in the material. UHPFRC has high compressive strength of up to 200 MPa and tensile strength of about 20–40 MPa. In addition, the fracture energy of UHPFRC can be about 20,000–40,000 J/m^2, which is several orders of magnitude higher than that of normal concrete materials [10]. Therefore, UHPFRC has much higher resistance to high strain rate loading than normal concrete. Some full scale tests have been carried out in this field and results demonstrated that under the same blast loading, UHPFRC performed much better than normal strength concrete [11–13].

In order to better understand the behaviour of UHPFRC under different blast loading, more blast tests are required, including full scale blast tests and small specimen blast tests. However, although a full scale test can better express actual structural behaviour, it is time-consuming and costly, while specimen based test is easy to perform, but results from them may be different from real size structures due to size effect. Moreover, as UHPFRC contains high fibre volume, the variation of fibre orientation will also cause differences in UHPFRC behaviour, even for specimens with the same fibre volume; this further increases the complexity of understanding UHPFRC behaviour from tests. Reliable modelling is therefore an alternative important tool to study UHPFRC behaviour when subjected to high strain rate loading. The developed model should express the properties of the studied structure, including strengths, stress–strain curve, size effect if difference in dimension exists between test specimen used to obtain material properties

* Corresponding author. Tel.: +44 79 8574 9226.
E-mail address: lei.mao@port.ac.uk (L. Mao).

0734-743X/$ – see front matter © 2013 Elsevier Ltd. All rights reserved.
http://dx.doi.org/10.1016/j.ijimpeng.2013.10.003

and modelled structures. Moreover, the model should also capture strain rate effect in the structure to simulate material and structural behaviour under high strain rate loading conditions.

According to previous studies, only limited research has been carried out to model UHPFRC under blast loading [12,14]. In these studies, only the maximum deflection was predicted from the models, while the damage to the UHPFRC after blast loading could not be predicted. The reason is that in most studies, UHPFRC behaviour was predicted with a single degree of freedom (SDOF) model, where the failure model could not be obtained. In other models for UHPFRC, like those implemented in Autodyn and LS-DYNA, the stress–strain curve of UHPFRC, especially the strain softening phase, was not fully captured with the models and strain rate effect of UHPFRC is not fully understood and applied to the models. Therefore, modelling of UHPFRC under blast loading should be further studied, so that actual behaviour of UHPFRC, including both deflections and damage, can be predicted reliably.

This paper investigates the capability of modelling UHPFRC behaviour under blast loading using the explicit non-linear finite element program, LS-DYNA [15], and clarifies effect of steel fibre and reinforcement bars in providing blast resistance of UHPFRC through numerical studies. It should be mentioned that in order to better distinguish these two effects, the effect of fibre orientation, which would also cause difference in UHPFRC behaviour, was not considered in the study. Steel fibre was not modelled explicitly in the model and its effect is expressed by matching stress–strain curve of model to that from actual UHPFRC specimen. In Section 2, the key features of the concrete damage model that was used in the study are presented and the use of a typical stress–strain relationship for UHPFRC to determine model parameters based on the internal automatic parameter generation is described. A brief description of the experimental blast tests is provided, published in greater detail elsewhere [14,16]. In the modelling analysis, the determined model parameters were used to predict the behaviour of the UHPFRC panels under blast loading and the predicted results, including the panel deflections and damage, are compared to the test data. Furthermore, with the validated models, parametric studies were carried out to investigate the effectiveness of bar reinforcement and steel fibre in providing resistance of UHPFRC to blast loading. Finally, some conclusions are given.

2. Concrete damage model in LS-DYNA

The concrete damage model, also known as Karagozian & Case (K&C) concrete model, was firstly developed for DYNA3D, and later available in LS-DYNA as Material #72. It has been widely used to analyse concrete response to blast loading due to its simple implementation [17–19]. In the K&C model, two methods can be used to provide model parameters. The first method is by inputting detailed material properties directly into the model, enabling the actual behaviour of material to be captured with reasonable accuracy. However, this method requires large numbers of material characterization tests for providing material properties. In the second method, only the concrete compressive strength is required as input, and all other related parameters are calculated with the embedded automatic parameter generation method. This method does not need a series of material characterization tests, but as the parameter generation method is based on test data from normal strength concrete, in order to apply this method to other concrete materials, further modifications to the model parameters should be performed to let the model better express the behaviour of actual material, such as stress–strain relationship.

In the concrete damage model, the strain hardening and softening behaviour can be expressed with properly configured model parameters and the strain rate effect can also be incorporated into the model, where the strength enhancements in compression and tension can be defined separately.

Based on previous studies employing the K&C model for simulating concrete behaviour [20,21], it can be found that the K&C model is mostly used to predict behaviour of normal strength concrete, where the automatic parameter generation method can be used directly without further modifications to model parameters. However, limited studies have been devoted to model high strength concrete materials with the K&C model, thus the performance of the K&C model after modifying model parameters for predicting high strength concrete behaviour remains unclear.

2.1. Strength surfaces

The concrete damage model uses a simple function for the definition of three independent strength surfaces, including the initial yield, maximum failure and residual surfaces. These surfaces can be expressed as:

$$F_y(p) = a_{0y} + \frac{p}{a_{1y} + a_{2y}p} \tag{1}$$

$$F_m(p) = a_{0m} + \frac{p}{a_{1m} + a_{2m}p} \tag{2}$$

$$F_r(p) = \frac{p}{a_{1r} + a_{2r}p} \tag{3}$$

where p is the pressure, and F_y, F_m and F_r represent the initial yield, maximum failure and residual surfaces, respectively [18].

The plasticity surface is interpolated between the initial yield and maximum failure surfaces to represent the strain hardening, which can be written as:

$$F_h = \eta F_y + (1-\eta)F_m \tag{4}$$

Similarly, for representing strain softening, another surface is interpolated between the maximum failure and residual surfaces, which is expressed as:

$$F_s = \eta F_y + (1-\eta)F_r \tag{5}$$

where η is defined as the yield scale factor, and is the function of the effective plastic strain measure λ:

$$\lambda = \begin{cases} \int_0^{\overline{\varepsilon_p}} \dfrac{d\overline{\varepsilon_p}}{[1+p/f_t]^{b_1}} & p \gg 0 \\ \int_0^{\overline{\varepsilon_p}} \dfrac{d\overline{\varepsilon_p}}{[1+p/f_t]^{b_2}} & p < 0 \end{cases} \tag{6}$$

where $d\overline{\varepsilon_p}$ is effective plastic strain increment, f_t is the quasi-static concrete tensile strength.

From Equations (4)–(6), it can be seen that in the concrete damage model, b_1 and b_2 are employed to control the concrete hardening and softening behaviours. Thus the concrete behaviour, especially the strain softening behaviour, can be configured based on actual concrete behaviour by changing these two parameters, as investigated in the next section.

Table 1
Key stress and strain values in Fig. 1.

Model parameter	Value
a_{0y}	50.25
a_{1y}	0.45
a_{2y}	4.75E-4
a_{0m}	37.94
a_{1m}	0.63
a_{2m}	1.51E-3
a_{1r}	0.44
a_{2r}	6.96E-4
b_1	1.6
b_2(default)	1.35
b_2(modified)	−2

Table 2
Determined model parameters.

Tension		Compression	
Tensile strength ($f_{d,t}$) Of panels A, B and C	10 MPa	Compressive strength ($\sigma_{c,p}$) of panels A, B and C	170 MPa
Tensile strength ($f_{d,t}$) of Panel D	15 MPa	Compressive strength ($\sigma_{c,p}$) of Panel D	190 MPa
Max linear strain ($\varepsilon_{t,1}$)	0.00011	Max linear strain ($\varepsilon_{c,1}$)	0.0031
Limiting tensile strain ($\varepsilon_{t,p}$)	0.004	Limiting compressive strain ($\varepsilon_{c,p}$)	0.004
Max tensile strain ($\varepsilon_{t,u}$)	0.01	Max compressive strain ($\varepsilon_{c,u}$)	0.007

2.2. Determination of model parameters

From above, it can be seen that a number of parameters should be determined to express the model behaviour. According to Eqs. (1)–(3), eight parameters are required to define three independent surfaces. a_{0y}, a_{1y} and a_{2y} can be determined based on experimental data from a uniaxial unconfined compression test and some confined compression tests, while the definition of maximum and residual surfaces also requires appropriate test data. In this study, since only limited material properties are available, the automatic parameter generation method in K&C model was employed, which is derived using data from larger numbers of material characterization tests and previously derived data [22]. These values, which are calculated automatically with compressive strength of 170 MPa, are listed in Table 1.

However, as the automatic parameter generation in the K&C model is based on test data from normal strength concrete materials with uniaxial compressive strength of 45 MPa [23], it may not represent the actual behaviour of UHPFRC material, which has much higher strengths (compressive strength of 170 MPa in this study). Therefore, before using the automatically generated parameters for the analysis of UHPFRC, it is necessary to study the capability of automatically generated parameters in expressing the behaviour of UHPFRC.

In the study, the stress–strain relationship of UHPFRC shown in Fig. 1 was used to investigate the capability of the K&C model in describing the behaviour of UHPFRC. Some key stress and strain values from this relationship are listed in Table 2. Note that the two different values of compressive and tensile strength shown in Table 1 relate to the two UHPFRC mixtures used in the experimental work which had different fibre contents (see below for further details). The tensile and compressive strength values were obtained from quasi-static tests published elsewhere [12].

Some research has been devoted to perform UHPFRC tension tests and investigate the effect of fibres on UHPFRC behaviour. Results demonstrate that variation of fibre volume in UHPFRC could affect its tensile behaviour significantly, while the effect is minor in compressive behaviour [24,25]. With the developed model, a sensitivity analysis was performed to investigate the effect of compressive and tensile properties and results showed that the behaviour of UHPFRC panels under blast loading was dominated by their tensile properties, as changes in compressive properties did not affect UHPFRC performance significantly. Therefore, in this study, the modelled stress–strain relationship under tension was studied and compared to the designed stress–strain relationship shown in Fig. 1.

It should be mentioned that this relationship is an idealized curve (ideal trapezoidal shape), while stress–strain curves from tests did not show such a flat strain hardening phase. It was also observed from tests that variation in fibre orientation would clearly affect the shape of the stress–strain curve [10]. However, as it is difficult to control the test after UHPFRC fracture, as it would rupture abruptly after fracture, strain softening phase of the stress–strain curve was not be measured from tests. Therefore, in this study, the idealized curve is employed for configuring the model and size effect is not considered.

In order to obtain the stress–strain curve from the model, a single element analysis was carried out. In the analysis, the bottom surface of the element was constrained, and a uniaxial tensile stress was applied to the top of the element until the complete fracture of the element. From the results, the elemental stress could be obtained directly, while the strain was calculated as displacement of the top of the element divided by the element height. Fig. 2 depicts the comparison of the results of modelled stress–strain curve using automatic generated parameters and the idealized relationship. It can be seen that the generated stress–strain curve from the model shows higher ductility than the designed behaviour.

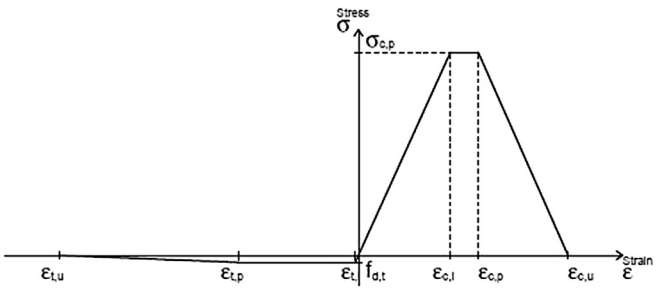

Fig. 1. Designed stress–strain relationship of UHPFRC.

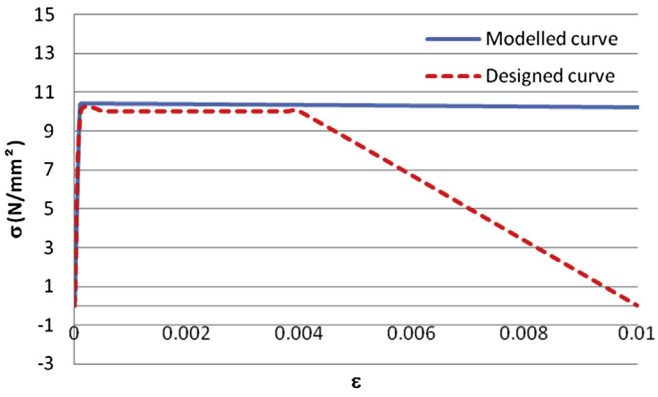

Fig. 2. Comparison of stress–strain relationship under tension with default b_2 value.

From the above results, it can be concluded that the model with automatically generated parameters could not represent the actual behaviour of UHPFRC panels. According to Eqs. (4)–(6), the target fracture energy can be achieved by adjusting the value b_2, and the stress–strain relationship of the model, especially the strain softening behaviour, can thus be modified to match the designed relationship. b_2 was therefore adjusted so that the modelled stress–strain relationship produced by the single element analysis closely matched the designed stress–strain curve and the comparison is shown in Fig. 3.

From Fig. 3, it can be seen that after modification of b_2, the modelled stress–strain curve matches better to the idealized curve, although the hardening behaviour still cannot be expressed clearly in the modelled curve.

It should be mentioned that for different element sizes, the b_2 value should be changed accordingly in order to obtain the same stress–strain relationship. The reason is that with the variation of element size, the stress–strain relationship will be changed, which is shown as follows [19,23]:

$$\int \sigma d\varepsilon = G_f/h_c \tag{7}$$

where G_f is the tensile strain energy, h_c is the element size.

Table 2 summarizes the model parameters used in the model; in the table both default and modified values of b_2 are listed.

2.3. Strain rate effect

In the concrete damage model, the strength enhancement is implemented along a radial stress path and the maximum failure surface F_m and effective plastic strain λ are employed to represent the rate effect. Since the strain rate effect is expressed with the enhanced strengths in compression and tension tests, the scale factor r is defined as follows:

$$r = \frac{f_{c,\text{new}}}{f_{c,\text{old}}} \tag{8}$$

where f_c is the unconfined compressive strength of concrete.

The modified maximum failure surface is then obtained:

$$F_{\text{new}} = a_{0,\text{new}} + \frac{p}{a_{1,\text{new}} + a_{2,\text{new}} p} \tag{9}$$

where $a_{0,\text{new}} = ra_0$, $a_{1,\text{new}} = a_1$, $a_{2,\text{new}} = a_2/r$.

The effective plastic strain λ should also be adjusted to incorporate strain rate effect in evaluating the damage, thus Eq. (6) is modified as:

$$\lambda = \begin{cases} \int_0^{\overline{\varepsilon_p}} \dfrac{d\overline{\varepsilon_p}}{r[1+p/rf_t]^{b_1}} & p \gg 0 \\ \int_0^{\overline{\varepsilon_p}} \dfrac{d\overline{\varepsilon_p}}{r[1+p/rf_t]^{b_2}} & p < 0 \end{cases} \tag{10}$$

As described above, when subjected to high strain rate loading, the strain rate effect should be considered to properly analyse the concrete behaviour. According to previous studies, rate effect in concrete is due to moisture at low strain rate and inertia effect at high strain rate, so the proper way of expressing rate effect is for the model to capture the inertia effect. According to previous studies [17,18], in the numerical model, the inertia effect in compression can be captured from the mass of the outer cylinder elements resisting motion laterally, and inertia effect in tension can be expressed by capturing aggregate interlocking that propagates the micro-cracking and energy dissipation beyond the localization zone. However, in the concrete damage model, the inertia effect in tension cannot be captured so in this study, the strain rate effect was incorporated by inputting the dynamic increase factors (DIF) at different strain rates. It should be mentioned that this method will lead to uncoupling of concrete hydro effect, and when obtaining DIF values from tests, radial confinement and friction should be considered to let DIF value represent actual rate effect. Moreover, from previous results [18], with various element sizes, similar DIF values would be obtained at same strain rate, which means element size will not affect the calculation of strain rate. Therefore, in this study, with selected element size, fracture energy is adjusted to match the design value (from design stress–strain curve), while DIF values are fixed.

Based on previous results [12,26], the variation of DIF value with strain rate under compression and tension can be expressed as:

$$\text{Compression DIF} = \begin{cases} \left(\frac{\dot{\varepsilon}}{\dot{\varepsilon}_s}\right)^{1.026\alpha} & \dot{\varepsilon} \ll \dot{\varepsilon}_1 \\ A_1 \ln(\dot{\varepsilon}) - A_2 & \dot{\varepsilon} > \dot{\varepsilon}_1 \end{cases} \tag{11}$$

where $\dot{\varepsilon}$ is strain rate, $\dot{\varepsilon}_s = 3 \times 10^{-5}\ \text{s}^{-1}$ is the quasi-static strain rate, $\alpha = 1/(20 + f_{cs}/2)$, f_{cs} is the static compressive strength, $\dot{\varepsilon}_1 = 0.0022f_{cs}^2 - 0.1989f_{cs} + 46.437$ ($\dot{\varepsilon}_1$ is 79 s^{-1} in this case), $A_1 = -0.0044f_{cs} + 0.9866$, $A_2 = -0.0128f_{cs} + 2.1396$.

$$\text{Tension DIF} = \begin{cases} \left(\frac{\dot{\varepsilon}}{\dot{\varepsilon}_s}\right)^{\delta} & \dot{\varepsilon} \ll 30\ \text{s}^{-1} \\ \beta\left(\frac{\dot{\varepsilon}}{\dot{\varepsilon}_s}\right)^{1/3} & \dot{\varepsilon} > 30\ \text{s}^{-1} \end{cases} \tag{12}$$

where $\dot{\varepsilon}_s = 10^{-6}\ \text{s}^{-1}$, $\log\beta = 7.11\delta - 2.33$, $\delta = 1/(10 + 6f_{cs}/f_{co})$, f_{cs} is the static concrete compressive strength, $f_{co} = 10$ MPa.

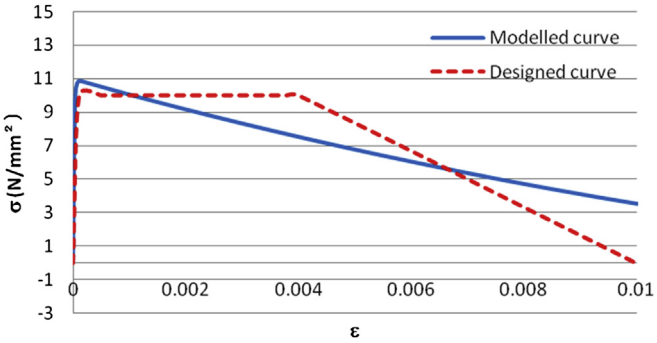

Fig. 3. Comparison of stress–strain relationship under tension with modified b_2 value.

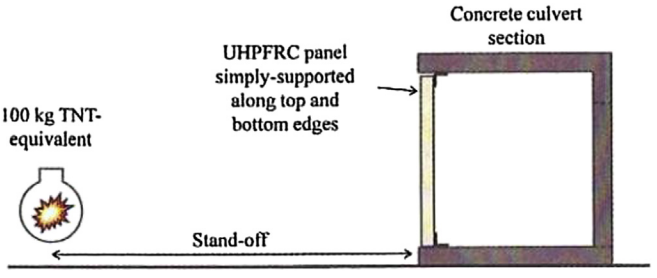

Fig. 4. Configuration of TNT charge and UHPFRC panel in the test (after Ref. [14]).

Table 3
Details of the four UHPFRC panels.

Panel	Fibres by volume		Steel reinforcement bar by volume	Stand-off distance
	13 mm long fibre	25 mm long fibre		
A	2%	0%	3.4%	9 m
B	2%	0%	3.4%	7 m
C	2%	0%	0.3%	12 m
D	2%	2%	0.3%	12 m

From Eq. (11), it can be seen that under compression, the critical strain rate ε_1, at which there is a sudden increase in DIF value, varies with the concrete static compressive strength. This is consistent with test results using different strength concretes [27]. When compared to test data from the UHPFRC under compression tests [28], the DIF values obtained using Eq. (11) are comparable to the DIF values from tests. Therefore, Eq. (11) can be employed to express reasonable strain rate effect of UHPFRC under compression.

However, under tension, the variation of critical strain rate with concrete strength is still under investigation. Thus, in this study, the critical strain rate is fixed at 30 s^{-1} regardless of concrete strength based on the CEB code.

3. Full scale blast tests on UHPFRC panels

3.1. Set-up of UHPFRC panels and TNT charge

Blast tests on UHPFRC panels were conducted in July 2008 at GL Industrial Services, Spadeadam, Cumbria. The arrangement of the panel and explosive charge is depicted in Fig. 4. In the test, the top and bottom edges of the panel were simply supported. The blast load was generated by 100 Kg TNT-equivalent placed at an appropriate stand-off distance.

Four panels with dimensions of 3.5 m × 1.3 m × 0.1 m were employed in the test, having different fibre and steel reinforcement bar volumes and different stand-off distances. The details of the panels are listed in Table 3. It should be mentioned that according to previous studies [10], fibre orientation will clearly affect the flexural properties of UHPFRC, thus response of UHPFRC under blast loading will be influenced by fibre orientation and distribution. Panels were cast side-on so any variation in fibre distribution due to segregation of the mixture would be across the width of the panel rather than in the vertical direction. However, as the aims of this study were to investigate the performance of the K&C model in simulating UHPFRC behaviour and to use the numerical model to clarify steel fibre and reinforcement bar effect in improving blast resistance of UHPFRC steel fibres were not simulated explicitly, in order to reduce the complexity of the model and distinguish these two effects more clearly. The models were developed based on an idealized stress–strain curve for UHPFRC, so the effects of fibres on

Fig. 5. The broomstick device in the test.

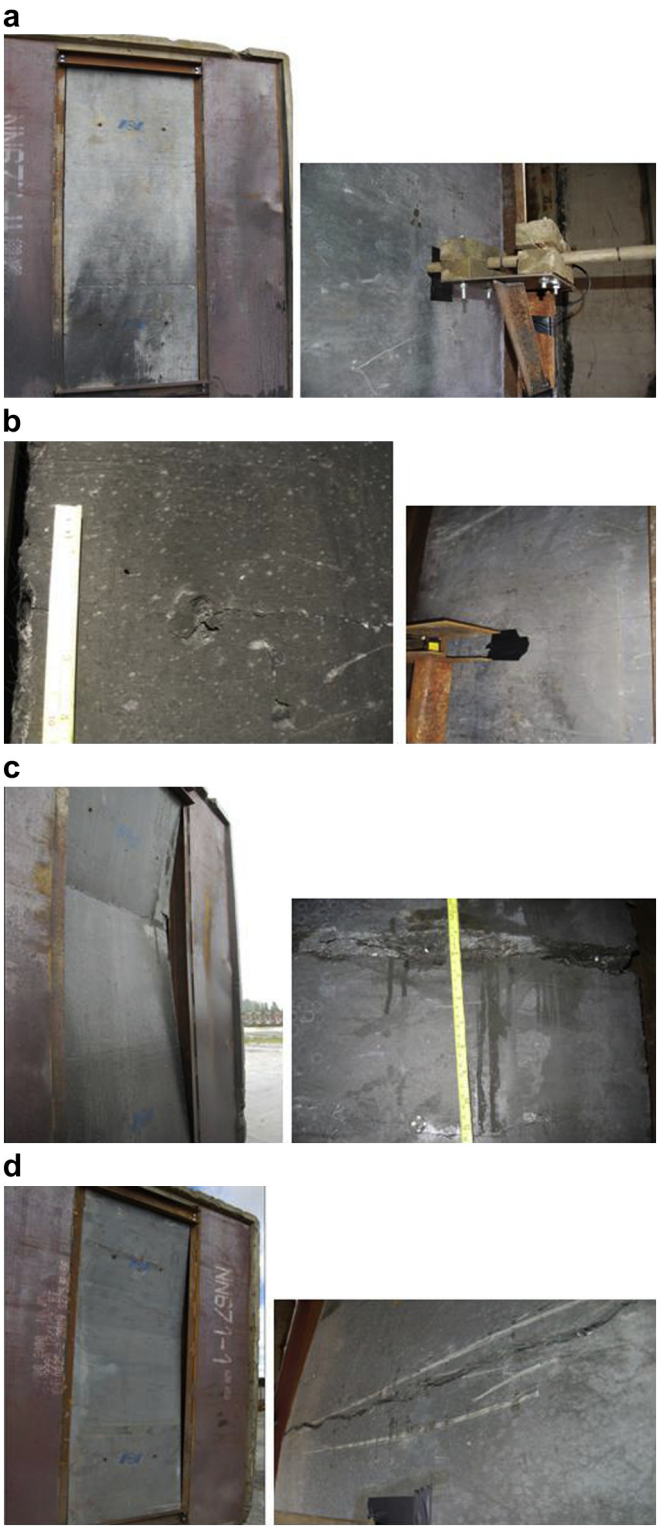

Fig. 6. The tested four panels after blast load. (a) The front and rear faces of panel A after blast load. (b) The front and rear faces of panel B after blast load. (c) The front and rear faces of panel C after blast load. (d) The front and rear faces of panel D after blast load.

Table 4
Recorded maximum and permanent mid-span deflection of four panels.

Panel	Maximum mid-span deflection (mm)	Permanent mid-span deflection (mm)
A	110	20
B	210	50
C	180	180
D	90	90

the behaviour of the material are incorporated through the stress–strain behaviour.

In the test, data were collected to evaluate the performance of UHPFRC panels under blast loading. The blast reflected pressure was recorded at 12 m distance from the charge using gauges mounted on a separate concrete culvert facing the blast wave. For 7 m and 9 m stand-off distances, the pressure data were not collected due to risk of damage to the equipment. Laser gauges were placed on the rear face of panels A and D to obtain the panel deflection. In addition, the panel peak and permanent deflections were also measured using a simple broomstick device, which is shown in Fig. 5. It should be mentioned that all deflection measurements were at mid-span of the panels; they may not the maximum deflection as the fracture is not symmetric. Strain rates calculated from deflection data were $\sim 1\ s^{-1}$.

3.2. Blast test results

Fig. 6 shows the four panels after the blast loads. It can be observed that in panel A (Fig. 6a), which has higher steel reinforcement bar volume, only minor horizontal cracks appeared on the front and rear panel faces. Furthermore, even with a closer explosion, panel B still had only a small permanent deflection, although more horizontal cracks appeared on the rear face of the panel (Fig. 6b). However, for panel C, which has lower steel reinforcement bar volume, a severe crack (shown in Fig. 6c) was observed after the blast loading. With more added fibres, panel D (Fig. 6d) experienced smaller deflection than that of panel C, but the blast load also caused a large permanent deflection and large crack in the panel. These observations can be confirmed with the recorded maximum and permanent panel deflections, which are listed in Table 4. Therefore, it can be concluded that the steel bar reinforcement greatly improved the resistance of UHPFRC panels to the blast load with 7 m and 9 m stand-off distances, and increasing the amount of steel fibres also increased the panel resistance to a certain degree under blast load with 12 m stand-off distance The relative effects of bar and fibre reinforcement are discussed further in Section 5.

It should be mentioned that for panels C and D, the large cracks appeared at a position above the panel mid-span. This was also observed in the models described below. Models with the charge at different heights showed that the fracture position would also be changed accordingly, thus this non-symmetric panel fracture is caused by non-uniform blast loading applied to the panel as a result of ground reflection of blast wave. In the tests and in the models presented below, the charge was positioned 1 m above the ground.

Table 5
Material properties of UHPFRC panel.

Properties	Value
Static compressive strength of concrete	170 MPa
Static tensile strength of concrete	10 MPa
Density of concrete	2450 kg/m^3
Young's modulus of steel reinforcement	200 GPa
Yield strength of steel reinforcement	1680 MPa

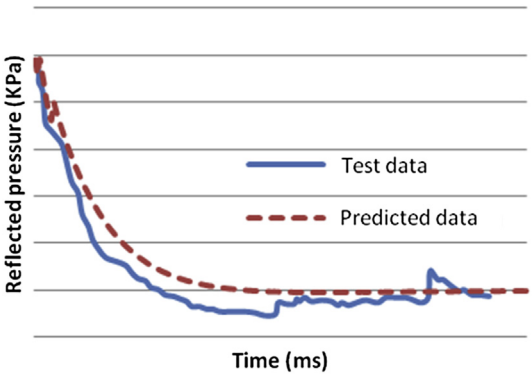

Fig. 7. Comparison of reflected pressure at 12 m.

4. Modelling of UHPFRC panels under blast loading

4.1. Development of model

In the study, the model of the UHPFRC panel was developed based on actual dimension and boundary conditions. It should be mentioned that since the large concrete culvert acted as a rigid body in the test, it was not included in the model and the actual boundary condition was achieved by constraining both translations and rotations of panel top and bottom edges.

The UHPFRC panel was modelled using the concrete damage model with the modifications described above, and equation of state 8 (EOS 8) in LS-DYNA was employed in the study to give the relationship between pressure and volumetric strain.

In the UHPFRC model, the element size of the UHPFRC model was 20 mm × 20 mm × 5 mm. A mesh convergence study was carried out to verify the selected element size could give convergence results for UHPFRC panel.

For panels A and B, the steel reinforcement was simulated with *MAT_PLASTIC_KINEMATIC model in LS-DYNA, and rate effect in reinforcement bars is not considered in this study. The bond behaviour between the concrete and reinforcement was achieved by sharing nodes between concrete and reinforcement elements in the model. Table 5 lists the mechanical properties of the UHPFRC and steel reinforcing bar.

4.2. Modelling results

The developed model was used to model the behaviour of UHPFRC panels under blast loading. The results from the model were then compared to the test data as shown below.

In the modelling, the blast load was modelled using *LOAD_BLAST in LS-DYNA. Blast reflected pressures from the model were obtained as the sum of nodal forces applied to the panel divided by area of panel face subjected to the blast wave, and are compared to the test data for a stand-off distance of 12 m in Fig. 7. It can be seen that both peak blast pressure and blast impulse were predicted with good quality. It should be mentioned that in the current study, the sampling interval for obtaining blast pressure from model is 0.1 ms. In order to confirm that the selected sampling interval can give reasonable blast pressure and express UHPFRC panel behaviour, two other sampling intervals, 0.01 ms and 1 ms, were used to obtain blast pressure, and corresponding panel deflections were also studied, which were depicted in Fig. 8.

From above figure, it can be observed that with 0.01 ms and 0.1 ms sampling intervals the same blast pressure and panel deflection can be obtained, while with 1 ms sampling interval, blast pressure shows small variation due to limited sampling points, but

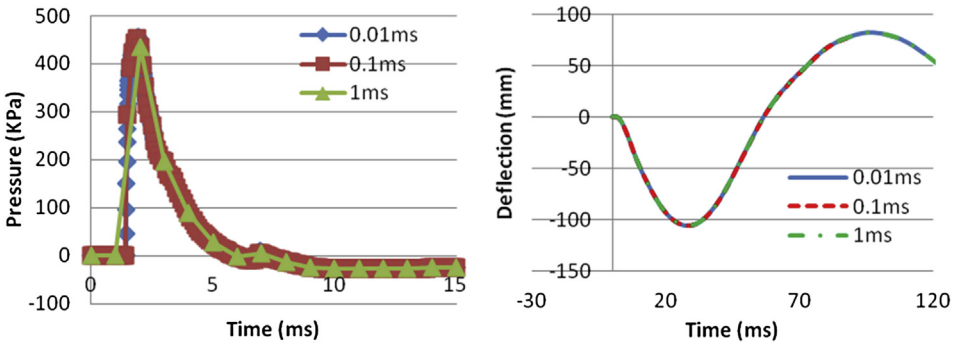

(a) Blast pressure (b) Panel deflection

Fig. 8. Modelled blast pressure and panel deflection with various sampling intervals.

panel deflection can still be obtained with good quality. Therefore, based on modelling results, with 0.1 ms sampling interval, the actual blast pressure can be fully captured.

Fig. 9 shows the comparison of results for panel A deflections from test data and the developed model. It can be seen that both forward and backward maximum mid-span deflections from the model are in good agreement with the test data.

However, the predicted damage of panel A showed a larger difference from the observations in the test. More cracks appeared on panel A from the model, as shown in Fig. 10, while only minor cracks on the rear panel face are observed from the test data (shown in Fig. 6a). Similar failure mode was observed by Tu and Lu [19], where the response of a normal strength concrete panel subjected to blast loading was simulated with MAT72 and RHT models and the results indicated that multiple cracks existed in the slab after the blast loading.

It should be mentioned that the fringe levels used in Fig. 10 represent the effective plastic strain λ (shown in Eq. (6)), which is used to evaluate damage in the model. According to previous studies [4,17,18,29], the primary damage exists when the effective plastic strain is larger than 1.95, while secondary damage can be represented with effective plastic strain between 1.8 and 1.95. However, as those effective plastic strain values causing primary damage are obtained by comparing model failure and actual structural failure from tests, they may not represent actual damage level of UHPFRC structures, further investigation of effective plastic strain and corresponding actual damage level, especially for UHPFRC, should be performed.

The difference in the damage levels between model and blast tests could be attributed to the lack of systematic investigation of effective plastic strain and corresponding actual damage in UHPFRC, which may not evaluate actual damage levels with the effective plastic strain value. It is also possible that in the experimental tests, some cracks may close up during the rebound of panels, so that they cannot be observed after the test and the damage is more extensive than is suggested by visual inspection of the exterior. X-ray CT imaging techniques could be employed to check the concrete's internal condition and thus better evaluate the concrete damage.

Figs. 11 and 12 depict the predicted deflection and damage of panel B. It can be seen that the maximum and permanent

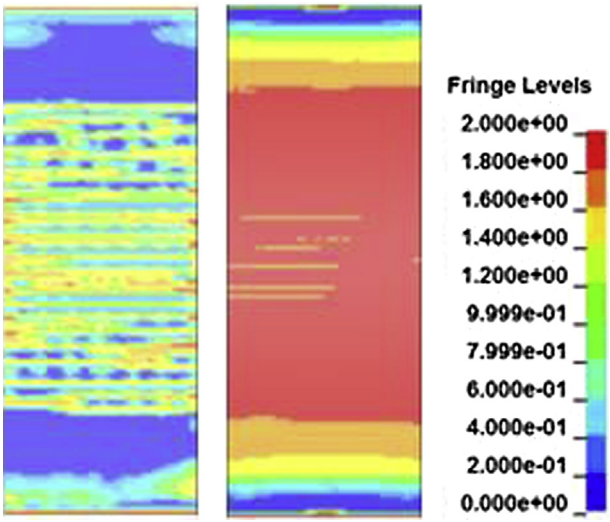

Fig. 10. Predicted damages on front (left) and rear (right) faces of panel A.

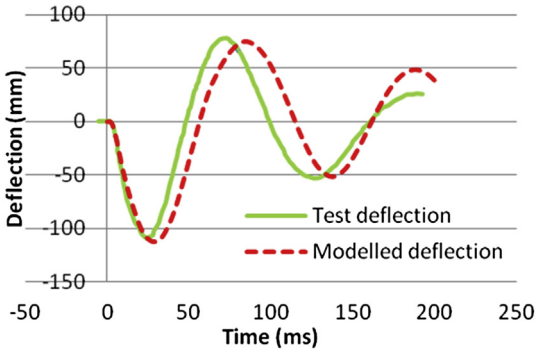

Fig. 9. Comparison of results of panel A deflection.

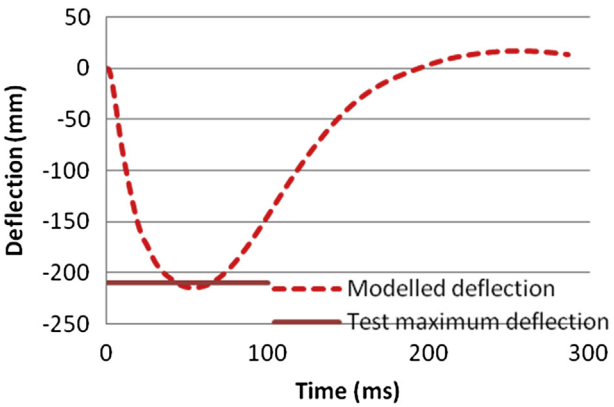

Fig. 11. Predicted deflection of panel B.

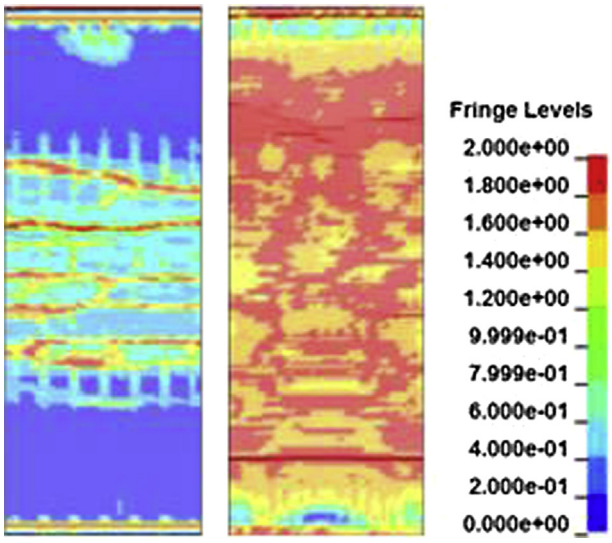

Fig. 12. Predicted damages on front (left) and rear (right) faces of panel B.

deflections of panel B are 216 mm and 18 mm, respectively, which are consistent with the test data in Table 4. Several horizontal cracks appear on the rear panel face, which also match the observations shown in Fig. 6b.

The deflection of panel C from the model is depicted in Fig. 13. The maximum and permanent predicted deflections are 220 mm and 210 mm, respectively, which are reasonable when compared to test data in Table 4. Moreover, the observed damage in Fig. 6c also validates the predicted damage from the model, which is shown in Fig. 14.

The modelling results from panel D were also obtained and compared to the test data. Figs. 15 and 16 show the comparison of panel deflection and predicted damage, respectively. From the results it can be observed that both predicted panel deflection and damage are consistent with test data.

Finally, the comparison of maximum and permanent mid-span panel deflections is summarized in Table 6. From the results it can be concluded that with the UHPFRC behaviour under blast loading can be predicted with good quality using the concrete damage model after matching stress–strain curve from the model to that of UHPFRC specimen.

5. Investigation of effectiveness of steel bar reinforcement and steel fibres in UHPFRC

After validating the developed model, parametric studies were carried out to investigate the effectiveness of steel bar

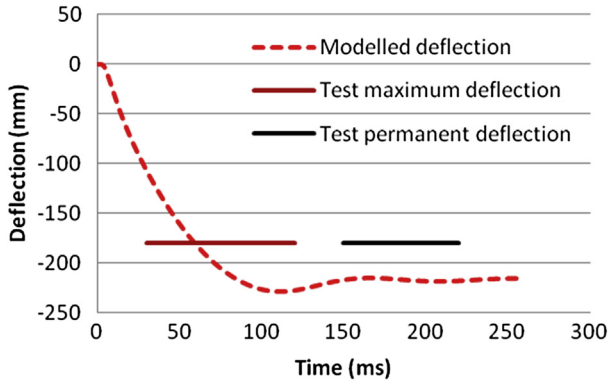

Fig. 13. Predicted deflection of panel C.

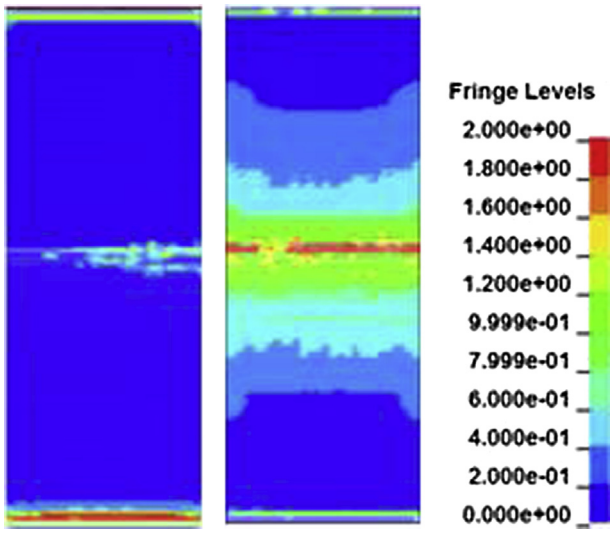

Fig. 14. Predicted damages on front (left) and rear (right) faces of panel C.

reinforcement and steel fibres in UHPFRC, especially in providing extra resistance to the UHPFRC panels under different blast loading conditions.

According to the results in Sections 3 And 4, it can be seen that increasing the density of steel bar reinforcement can greatly improve the resistance of UHPFRC when subjected to blast loading. Moreover, the UHPFRC resistance to blast loading was also improved in panel D (which contained a mixture of 2 fibre types with total fibre volume of 4%) compared to panel C which contained 2% by volume of a single type of fibre. In order to better understand these effects under different blast conditions, parametric studies were carried out with the above validated models.

In the study, the blast load was generated from a fixed 100 kg TNT-equivalent charge. Different stand-off distances were used, so that various scaled distances Z could be obtained to include different loading regimes [30]:

$$\begin{aligned} &\text{Close in}: \quad Z \ll 1.2\ \text{m/kg}^{1/3} \\ &\text{Near field}: \quad 1.2\ \text{m/kg}^{1/3} \ll Z \ll 3.97\ \text{m/kg}^{1/3} \\ &\text{Far field}: \quad Z > 3.97\ \text{m/kg}^{1/3} \end{aligned} \tag{13}$$

In the study, panels A, C and D are employed for the investigation. As for these two kinds of UHPFRC panels, all other parameters are the same except steel fibre and reinforcement bar volumes, which can be found in Table 3, this difference will cause change of

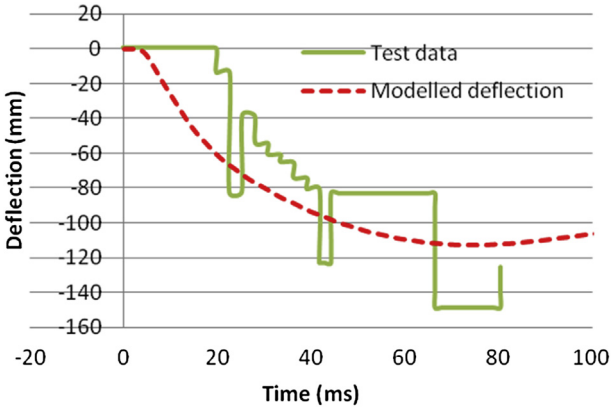

Fig. 15. Comparison results of panel D deflection.

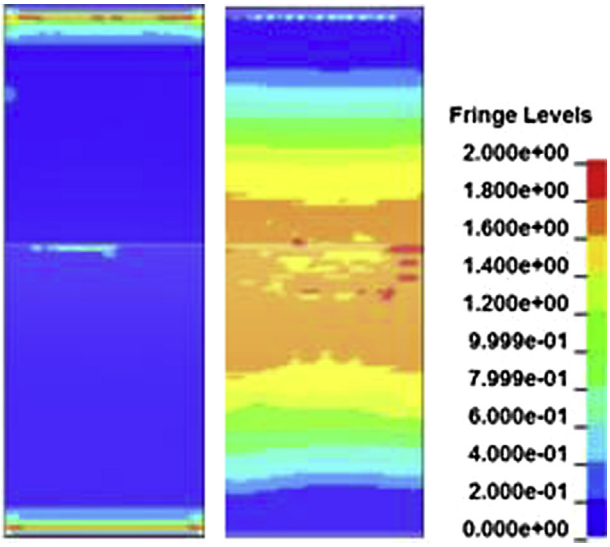

Fig. 16. Predicted damages on front (left) and rear (right) faces of panel D.

rate effect, inertial effect, tri-axiality of UHPFRC, thus will affect UHPFRC response under blast loading. By comparing results in panels C and D, the effect of steel fibre and reinforcement bar can be clarified. It should be mentioned that the increase of steel reinforcement and steel fibre volume are at a similar level (3% increase in bar reinforcement between panels C and A, and 2% in fibre reinforcement between panels C and D), thus the results from these three panels can be studied to compare the effects of steel bar reinforcement and steel fibres.

Fig. 16 depicts the results of parametric studies, which is expressed as the variation of maximum panel deflection with the scaled distance Z.

From the results it can be observed that, under far field blast loading ($Z > 3.3$ m/kg$^{1/3}$ in this case), the deflections from the three panels are similar, which indicates that the extra steel bar reinforcement and steel fibres do not provide clear extra resistance to the UHPFRC panel. When the blast loading is in the near field range ($Z < 3.3$), the additional steel fibres and reinforcement bar start to provide more resistance to the panel. This can be seen in Fig. 16 by the reduced deflections of panels C and D. When subjected to the blast loading with further reduced scaled distance ($Z < 2.7$ in this case), steel reinforcement bar becomes more effective in providing resistance to the panel, since the smallest maximum deflection can be found in panel A, which is shown in Fig. 17.

In order to further illustrate the effect of steel reinforcement bar and steel fibre, the panel deflections and damaged panels with $Z = 2.5$ are depicted in Fig. 18 and Fig. 19. From the figures it can be found that, with steel reinforcement bar, panel A experiences the smallest deflection and damage, which means in this case steel

Table 6
Comparison of maximum and permanent mid-span panel deflections.

Panel	Maximum mid-span deflection (mm)		Permanent mid-span deflection (mm)	
A	Test	110	Test	20
	Model	104	Model	–
B	Test	210	Test	50
	Model	216	Model	18
C	Test	180	Test	180
	Model	220	Model	210
D	Test	90	Test	90
	Model	110	Model	102

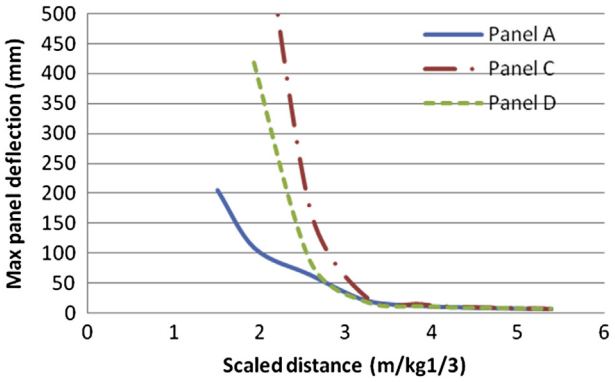

Fig. 17. Variation of maximum panel deflection with scaled distance from three panels.

reinforcement bar can provide panel resistance more effectively, while steel fibre can also provide certain amount of the resistance to the panel.

According to above results, when subjected to relative far blast loads ($Z > 2.7$ in the study), steel fibres and reinforcement bar have similar effects in increasing UHPFRC panel resistance. However, with close blast loads ($Z < 2.7$), the increased steel reinforcement volume can increase the panel resistance remarkably.

6. Conclusions

The concrete damage model in LS-DYNA was employed to model the behaviour of UHPFRC panels under blast loads. The automatic parameter generation method was used to generate model parameters and the stress–strain relationship of the model was further configured to match the designed stress–strain relationship of UHPFRC. Moreover, the strain rate effect was also incorporated in the model based on existing strain rate models for concrete.

With the modified model, the behaviour of UHPFRC panels under blast loads was obtained and compared to the corresponding test data. Results demonstrate that the peak blast pressure and blast impulse can be predicted with good quality from the model. Both the maximum and permanent deflection of the four panels tested could be obtained reliably, and damage of the panels after the blast loads can also be predicted with reasonable accuracy. As described before, the damage prediction can be improved by modelling the fibre explicitly in the concrete model, so that the fibre effect in bridging cracks can be expressed.

Furthermore, with the validated UHPFRC models, parametric studies were carried out to investigate the effect of steel bar

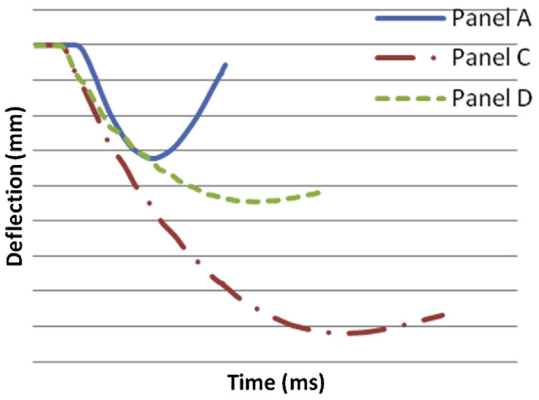

Fig. 18. Comparison of panel deflections with Z of 2.5.

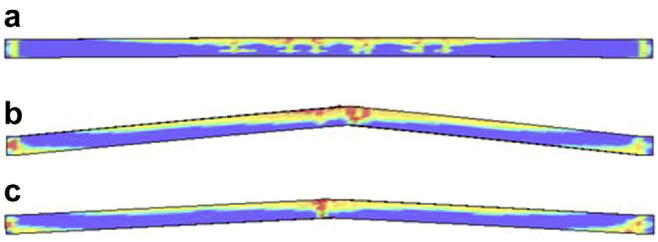

Fig. 19. Side view of panels after the same blast loading. (a) Panel A. (b) Panel C. (c) Panel D.

reinforcement and steel fibres in increasing UHPFRC resistance. From the results, it can be found that under far field blast loading, steel fibres and reinforcement bar are of similar effect in providing extra resistance to the UHPFRC panel. When subjected to near field blast loading, the resistance of UHPFRC panels can be increased significantly with steel reinforcement bar.

Acknowledgements

The authors are grateful to the Faculty of Technology and School of Civil Engineering and Surveying at the University of Portsmouth for financial support. The test data described here was collected as part of an EPSRC-funded project at the University of Liverpool. The authors gratefully acknowledge the significant contributions to this work by Professor Steve Millard (formerly University of Liverpool), Bekaert, VSL Australia, CPNI and GL Industrial Services.

References

[1] Bischoff PH, Perry SH. Compressive behaviour of concrete at high strain rates. Mater Struct 1991;24(6):425–50.
[2] Leppanen J. Concrete structures subjected to fragment impacts – dynamic behaviour and material modelling [Ph.D thesis]. Sweden: Chalmers University of Technology; 2004.
[3] Schenker A, Anteby I, Gal E, Kivity Y, Nizri E, Sadot O, et al. Full-scale field tests of concrete slabs subjected to blast loads. Int J Impact Eng 2008;35(3):184–98.
[4] Wang F, Wan YKMW, Chong QYK, Lim CH. Reinforced concrete slab subjected to close-in explosion. In: Proceedings of the second international workshop on performance, protection and strengthening of structures under extreme loading 2009. Hayama, Japan.
[5] Bhargava P, Sharma UK, Kaushik SK. Compressive stress-strain behaviour of small scale steel fiber reinforced high strength concrete cylinders. J Adv Concr Technol 2006;4(1):109–21.
[6] Dugat J, Roux N, Bernier G. Mechanical properties of reactive powder concretes. Mater Struct 1996;29(4):233–40.
[7] Lok TS, Zhao PJ, Lu G. Using the split Hopkinson pressure bar to investigate the dynamic behaviour of SFRC. Mag Concr Res 2003;55(2):183–91.
[8] Lok TS, ASCE M, Zhao PJ. Impact response of steel fiber-reinforced concrete using a split Hopkinson pressure bar. J Mater Civil Eng 2004;16(1):54–9.
[9] Garfield TT, Richins WD, Larson TK, Pantelides CP, Blakeley JE. Performance of RC and FRC wall panels reinforced with mild steel and GFRP composites in blast events. Procedia Eng 2011;10:3534–9.
[10] Barnett SJ, Lataste JF, Parry T, Millard SG, Soutsos MN. Assessment of fibre orientation in ultra high performance fibre reinforced concrete and its effect on flexural strength. Mater Struct 2010;43(7):1009–23.
[11] Gupta A, Mendis P, Ngo T, Lumantarna R. An investigation on the performance of structural components subjected to full-scale blast tests in Woomera, Australia. In: Performance, protection, and strengthening of structures under extreme loading 2007. Whistler, Canada.
[12] Ngo T, Mendis P, Krauthammer T. Behaviour of ultrahigh-strength prestressed concrete panels subjected to blast loading. J Struct Eng 2007;133(11):1582–90.
[13] Barnett SJ. Development of advanced concrete materials for anti-terrorism applications. Struct Eng 2008 October 7:28–9.
[14] Schleyer GK, Barnett SJ, Millard SG, Wight G, Rebentrost M. UHPFRC panel testing. Struct Eng 2011;89(23/24):34–40.
[15] Livermore Software Technology Corporation. LS-DYNA user's manual – version 971. Livermore, CA: Livermore Software Technology Corporation; 2007.
[16] Barnett SJ, Millard SG, Schleyer GK, Tyas A. Briefing: blast tests of fibre-reinforced concrete panels. Constr Mater 2010;163(3):127–9.
[17] Malvar LJ, Crawford JE, Wesevich JW, Simons D. A plasticity concrete material model for DYNA3D. Int J Impact Eng 1997;19(9–10):847–73.
[18] Malvar LJ, Crawford JE, Morrill KB. K&C concrete material model release III – automated generation of material model input. K&C Technical Report TR-99-24-B1. Glendale, CA. Livermore Software Technology Corporation; 2000.
[19] Tu ZG, Lu Y. Evaluation of typical concrete material models used in hydrocodes for high dynamic response simulations. Int J Impact Eng 2009;36(1):132–46.
[20] Tanapornraweekit G, Haritos N, Mendis P, Ngo T. Modelling of a reinforced concrete panel subjected to blast load by explicit non-linear FE code. In: Proceedings of earthquake engineering in Australia conference 2007 2007. Wollongong, NSW, Australia.
[21] Odeh AA. Modelling and simulation of bogie impacts on concrete bridge rails using LS-DYNA. In: 10th International LS-DYNA users conference 2008. Dearborn, Michigan, USA.
[22] Chen WF. Plasticity in reinforced concrete. New York: McGraw Hill; 1982.
[23] Magallanes JM, Wu Y, Malvar LJ, Crawford JE. Recent developments to release III of the K&C concrete model. In: Proceedings of the 11th international LS-DYNA user's conference 2010. Dearborn, MI.
[24] Hassan AMT, Jones SW, Mahmud GH. Experimental test methods to determine the uniaxial tensile and compressive behaviour of ultra high performance fibre reinforced concrete (UHPFRC). Constr Build Mater 2012;37:874–82.
[25] Kang ST, Lee Y, Park YD, Kim JK. Tensile fracture properties of an ultra high performance fibre reinforced concrete (UHPFRC) with steel fibre. Compos Struct 2010;92(1):479–85.
[26] Comite Euro-International du Beton (CEB-FIP). CEB-FIP model code 1990. Trowbridge, Wiltshire, UK: Redwood Books; 1990.
[27] Malvar LJ, Ross CA. Review of strain rate effects for concrete in tension. ACI Mater J 1998;95(6):735–9.
[28] Isaacs J, Magallanes J, Rebentrost M, Wight G. Exploratory dynamic material characterization tests on ultra-high performance fibre reinforced concrete. In: 8th International conference on shock & impact loads on structures 2009. Adelaide, Australia.
[29] Magallanes JM, Crawford JE, Wu Y. Modeling UHPC FRC materials using the K&C concrete model. In: 14th International symposium on the interaction and effects of munitions with structures (ISIEMS), Seattle, WA, September, 19–21, 2011 2011.
[30] Cormie D, Mays G, Smith P. Blast effects on buildings. 2nd ed. London, UK: Thomas Telford Limited; 2009.